desynaptic5 carries a spontaneous semi-dominant mutation affecting Disrupted Meiotic cDNA 1 in barley

Colas, Isabelle; Barakate, Abdellah; Macaulay, Malcolm; Schreiber, Miriam; Stephens, Jennifer; Vivera, Sebastian

Published in:
Journal of Experimental Botany

DOI:
10.1093/jxb/erz080

Publication date:
2019

Journal of Experimental Botany
doi:10.1093/jxb/erz080 Advance Access Publication 27 April 2019

RESEARCH PAPER

desynaptic5 carries a spontaneous semi-dominant mutation affecting *Disrupted Meiotic cDNA 1* in barley

Isabelle Colas[1], Abdellah Barakate[2,*], Malcolm Macaulay[1], Miriam Schreiber[1], Jennifer Stephens[1], Sebastian Vivera[2], Claire Halpin[2], Robbie Waugh[1,2,†] and Luke Ramsay[1,†]

[1] Cell and Molecular Sciences, The James Hutton Institute, Invergowrie, Dundee, Scotland DD2 5DA, UK
[2] Division of Plant Sciences, University of Dundee at The James Hutton Institute, Invergowrie, Dundee, Scotland DD2 5DA, UK

* Current address: Cell and Molecular Sciences, The James Hutton Institute, Invergowrie, Dundee, Scotland DD2 5DA, UK
† Correspondence: luke.ramsay@hutton.ac.uk or robbie.waugh@hutton.ac.uk

Received 14 December 2017; Editorial decision 13 February 2019; Accepted 28 February 2019

Editor: Zoe Wilson, University of Nottingham, UK

Abstract

Despite conservation of the process of meiosis, recombination landscapes vary between species, with large genome grasses such as barley (*Hordeum vulgare* L.) exhibiting a pattern of recombination that is very heavily skewed to the ends of chromosomes. We have been using a collection of semi-sterile *desynaptic* meiotic mutant lines to help elucidate how recombination is controlled in barley and the role of the corresponding wild-type (WT) meiotic genes within this process. Here we applied a combination of genetic segregation analysis, cytogenetics, and immunocytology to genetically map and characterize the meiotic mutant *desynaptic5* (*des5*). We identified an exonic insertion in the positional candidate ortholog of *Disrupted Meiotic cDNA 1* (*HvDMC1*) on chromosome 5H of *des5*. *des5* exhibits a severe meiotic phenotype with disturbed synapsis, reduced crossovers, and chromosome mis-segregation. The meiotic phenotype and reduced fertility of *des5* is similarly observed in *Hvdmc1*^{RNAi} transgenic plants and *HvDMC1*p:GusPlus reporter lines show DMC1 expression specifically in the developing inflorescence. The *des5* mutation maintains the reading frame of the gene and exhibits semi-dominance with respect to recombination in the heterozygote indicating the value of non-knockout mutations for dissection of the control of recombination in the early stages of meiosis.

Keywords: Barley, crossover, desynaptic, DMC1, immunocytology, meiosis, recombination, RNAi.

Introduction

Barley (*Hordeum vulgare* L.) is an inbreeding, diploid grass species with a 4.8 Gb genome organized into seven pairs of chromosomes (Mascher *et al.*, 2017). Typical of large genome cereals, recombination in barley is predominantly confined to the ends of chromosomes, restricting the reassortment of alleles in the extensive interstitial and proximal regions that contain up to 30% of the genes (International Barley Genome Sequencing Consortium *et al.*, 2012; Mascher *et al.*, 2017). This recombination landscape may be the result of various evolutionary drivers, including a potential need for maintenance of co-adapted gene complexes and epistasis in local adaptation (Brown *et al.*, 1980; Volis *et al.*, 2011). From a practical perspective this pattern of recombination will, however, potentially impede genetic progress in crop breeding programmes (Lambing *et al.*, 2017). A deeper understanding of meiosis in large genome plants will help us determine the constraints of genome structure and offer an opportunity to manipulate patterns of recombination. The latter is an emerging priority focused on addressing the

need for food security within increased environmental limitations (Able *et al*., 2009; Martinez-Perez, 2009).

The control of recombination and the interlinked processes of early meiosis have been intensively studied in model eukaryotic organisms and comparative studies undertaken in the model plant Arabidopsis (Baudat *et al*., 2013; Hunter, 2015; Mercier *et al*., 2015). Recent cytogenetic studies have extended this to barley with a description of meiotic progression and a chronology of meiotic events that, although largely conforming to expectations, highlight aspects of timing that are different from Arabidopsis (Higgins *et al*., 2012; Phillips *et al*., 2012). Further dissection of the underlying process would be enabled by the use of disruptive spontaneous or induced mutations and those generated via transgenesis of known meiotic genes (Barakate *et al*., 2014; Colas *et al*., 2016). In barley, 15 spontaneous and/or chemically/physically induced *desynaptic* mutations that were determined in the 1970s to have aberrant cytological meiotic phenotypes are available for this purpose (Lundqvist *et al*., 1997).

desynaptic5 (*des5*) was isolated as a spontaneous mutant in the barley cultivar Betzes that showed genetic semi-sterility (Hockett and Eslick, 1969). Early cytological studies indicated that *des5* has a severe meiotic phenotype with limited crossovers (CO) at metaphase I (8.1–10.6 univalents per cell) and lagging chromosomes and micronuclei at telophase I (Hernandes-Soriano, 1973). The meiotic phenotype is associated with severe sterility in the mutant with an ovule fertility estimated at 7% (Hernandes-Soriano, 1973). Using trisomic inheritance studies the mutation was provisionally mapped to either chromosome 5H or chromosome 7H (Hernandes-Soriano, 1973). Near isogenic lines (NILs) for all 14 *desynaptic* mutants were subsequently produced by recurrent backcrossing to the barley cultivar Bowman (Druka *et al*., 2011). Single nucleotide polymorphism (SNP) genotyping with 1384 SNPs (Illumina BOPA1) of BW243 (Bowman.*des5*) and the wild-type recurrent parent Bowman indicated that BW243 contained an 18.6 cM introgression in the central region of chromosome 5H (see Supplementary Fig. S1 at *JXB* online), as well as potential introgressions of 3.7 and 3.4 cM on the long arms of chromosomes 1H and 7H, respectively (Druka *et al*., 2011). Here, using a positional candidate-gene approach, we describe the identification and characterization of *DESYNAPTIC5* as the barley orthologue of the meiotic recombination protein DMC1.

DMC1 was initially described in yeast (Bishop *et al*., 1992) as a homolog of the bacterial strand exchange protein RECA and is highly conserved amongst eukaryotes, including plants (Bishop *et al*., 1992; Habu *et al*., 1996; Klimyuk and Jones, 1997; Doutriaux *et al*., 1998; Passy *et al*., 1999; Kathiresan *et al*., 2002; Devisetty *et al*., 2010). The recombinases DMC1 and RAD51 capture, for repair, the 3′ overhangs generated by resected double-strand breaks catalysed by SPO11, with RAD51 supporting invasion of a homologous DNA template by DMC1 (Sheridan *et al*., 2008; Da Ines *et al*., 2013; Du and Luo, 2013; Lorenz *et al*., 2014; Lichten *et al*., 2015; MacQueen, 2015). In mammals, *dmc1* mutants are deficient for synapsis and homologous pairing and lead to severe sterility due to prophase arrest (Pittman *et al*., 1998; Yoshida *et al*., 1998). In Arabidopsis, *dmc1* mutants also show abnormal synapsis, exhibit almost no recombination and chromosome anomalies, but are not completely sterile (Da Ines *et al*., 2012, 2013; Pradillo *et al*., 2012). In rice, the characterization of DMC1 is complicated by gene duplication driven by the evolutionarily recent chromosome 11 and 12 duplication (Ding *et al*., 2001; Nakashima *et al*., 2004) but OsDMC1 double mutants are sterile, exhibit abnormal synapsis, univalents at metaphase, and lagging chromosomes at anaphase I (Wang *et al*., 2016).

Although there have been a number of studies on DMC1 in other grasses, these have largely been phylogenetically or bioinformatically driven without functional studies to confirm DMC1's role (Shimazu *et al*., 2001; Mikhailova *et al*., 2006; Devisetty *et al*., 2010; Etedali *et al*., 2011; Barakate *et al*., 2014). Using super-resolution immunocytology we show that *des5* in barley has a deleterious effect on synapsis and crossing over, and that we can recapitulate the meiotic and semi-sterile mutant phenotypes using RNAi knockdowns in transgenic plants. This study represents the first functional study of DMC1 in a large genome cereal (barley) and provides additional evidence of the importance of early meiotic events in controlling meiotic COs in barley.

Materials and methods

Plant and material preparation

Barley cultivar (cv.) Bowman, Bowman near isogenic line BW243 (BC_3F_3 – *des5*) and populations derived from crossing BW243 to cvs Barke and Morex were grown in the glasshouse at 18 °C for 16 h light and 14 °C for 8 h dark. Barley cv. Golden Promise, *HvDMC1*^{RNAi}, ZmUBIp:GUSPlus and *HvDMC1*p:GUSPlus transgenic plants were grown in compost in a standard heated greenhouse under 16 h photoperiod with supplementary lighting provided by high pressure sodium vapour lamps (Powertone SON-T AGRO 400 W; Philips Electronic UK Ltd, Guildford, UK). For cytology, when plants were approximately 5–6 weeks old and had reached meiosis, anthers were staged and prepared as previously described for chromosome spread *in situ* hybridization (Colas *et al*., 2016) or immunocytology (Colas *et al*., 2017).

Mapping and sequencing

F_1 plants were produced from two crosses: BW243(*des5*) × cv. Barke and BW243(*des5*) × cv. Morex. These F_1 plants do not exhibit the sterility phenotype of BW243 and were selfed to produce F_2 populations. Ninety-six F_2 individuals from each cross were grown in a glasshouse under standard conditions (as above) and leaf tissue collected. The plants were grown until full maturity and the fertility of the plants was scored with the severe near-sterile phenotype acting as a proxy for homozygous *des5*. Frozen leaf material was disrupted in lysis buffer using a Qiagen grinder and DNA was extracted with Qiagen DNA extraction kits using an automated station, QIAxtractor® (Qiagen). Genetic mapping utilized a custom 384 SNP genotyping array using the Illumina BeadXpress platform on the two F_2 segregating populations, using segregation of the semi-sterile phenotype of *des5* as a Mendelian trait. Using JoinMap 4.0 (Kyazma) software, marker loci were assigned to linkage groups and two rounds of regression mapping used to order the loci within groups and maps drawn using Mapchart (Voorrips, 2002).

The genetically delineated region containing *des5* was studied for candidate genes using online tools (http://mips.helmholtz-muenchen.de/plant/barley/fpc/index.jsp). Primers were designed across the coding domain of prioritized candidate genes (see Supplementary Table S1). PCR products were sequenced using the BigDye v3.1 reaction kit and analysed on an ABI Prism 3730. For gene validation studies, mRNA was collected from 0.6 to 1.1 mm anthers (prophase I) and leaf tissue of

BW243 and Bowman using an RNA extraction kit (Qiagen) including DNase I treatment. cDNA was made using the standard protocol of the Superscript III kit (Life Technologies) and sequenced using specific primers encompassing the deleted region (Supplementary Table S2).

DNA in situ *hybridization*

Anthers were fixed in ethanol–acetic acid (3:1) for 24 h and stored in 70% ethanol at 4 °C until use. Slide preparation and DNA *in situ* hybridizations were performed as previously described (Colas *et al.*, 2016) by using a gentle squash method on coated slides (SuperFrost or Polysine). Hybridization mixture (50 µl) was applied to the sample, and slides were denatured at 70 °C on a hot plate (with coverslip) and moved to 37 °C overnight in a wet chamber. The sub-telomeric repeat HvT01 and the centromeric repeats (Jasencakova *et al.*, 2001) were labelled by nick translation with Biotin-dUTP and FITC-dUTP, respectively as previously described (Colas *et al.*, 2016).

Immunocytology

Plant material was fixed and prepared according to Colas *et al.* (2017). We used anti-TaASY1, a polyclonal antibody raised in rabbit against the wheat (*Triticum aestivum*) and barley protein ASY1 (Agrisera, UK) and anti-HvZYP1, a polyclonal peptide antibody raised in rat against the barley (*Hordeum vulgare*) protein ZYP1 (DC Biosciences, Dundee UK). Dilution and incubation time for anti-TaASY1 and anti-HvZYP1 were carried out as in Colas *et al.* (2017). For this study, we also developed a polyclonal antibody against HvDMC1 peptides. The barley anti-*HvDMC1* antibody was made in guinea pig by the company Dundee Cell Product (now DC Biosciences), UK. Two peptides, RVDFSGRGELAERQQKLA and DPKKPAGGHVLAHAATIR, were chosen from the HvDMC1 sequence (AF234170.1) and tested *in silico* for immunogenicity and synthetized. The purity of each peptide was tested at more than 80% by mass spectrometry and HPLC analysis. Individual peptides were coupled to KLH for immunization of animals and BSA for testing antisera. Immunization was done in two individual guinea pigs (one per peptide). Affinity purification of the anti-serum was done with assessment of the purified IgG using SDS-PAGE and Coomassie staining. Equal volumes of each peptide were premixed and then diluted at 1:200 in blocking buffer as per Colas *et al.* (2017). Secondary antibodies consisted of anti-rabbit (for ASY1), anti-rat (for ZYP1) and anti-guinea pig (for DMC1) labelled with with Alexa Fluor® (568, 488 and 633) (Life Technologies) diluted in blocking solution (1:300). Slides were washed in 1×PBS and mounted in Vectashield® containing 4′,6-diamidino-2-phenylindole (DAPI; H-1200, Vector Laboratories).

Microscopy and modelling

3D confocal stack images (512×512, 12 bits) were acquired with an LSM-Zeiss 710 using laser light of 405, 488, and 561 nm sequentially. Projections of 3D pictures and light brightness/contrast adjustment were performed with Imaris 8.0.2 (Bitplane). 3D-SIM images were acquired on a DeltaVision OMX Blaze (GE Healthcare) for laser light of 405, 488, and 564 nm as previously described (Colas *et al.*, 2016). Super-resolution 3D image stacks were reconstructed with SoftWorx 6.0 (GE Healthcare). 3D projection and surface modelling were performed with Imaris 8.0.2 (Bitplane). Foci counting was carried out manually using Fiji 1.51s plugin 'cell counter' and compared with manual counting in Imaris. Protein modelling was performed using the SWISS-MODEL workspace (Arnold *et al.*, 2006).

HvDMC1^{RNAi}, *ZmUBIp:GUSPlus and* HvDMC1p*:GUSPlus transgenic plants*

pBRACT214 vector (http://www.bract.org/constructs.htm#barley) was used to prepare pBRACT214m Gateway expression vector with a multi-cloning site (MCS) for the insertion of barley DMC1 (HvDMC1p) and maize ubiquitin (ZmUBIp) promoters. A list of oligonucleotides used for plasmid construct preparation can be found in Table S3.

ZmUbiquitin promoter was PCR amplified using the original pBract214 plasmid as template and the oligonucleotides ZmUBIpF and ZmUBIpR with *Stu*I and *Hin*dIII restriction sites, respectively. DMC1 promoter including the 5′-untranslated region (UTR) containing a small 93 bp intron (1579 bp in total) was PCR amplified using barley cv. Golden Promise genomic DNA as template and the oligonucleotides HvDMC1pStuI and HvDMC1pAscI. Both promoters were cloned, sequenced then released for insertion into the corresponding restriction sites of pBract214m.

GUSPlus coding sequence was amplified by PCR using two gateway oligonucleotides, attB1-GUSPlus and attB2-GUSPlus, and the plasmid pGPro8-PS2 (a gift from Dr Roger Thilmony, USDA-ARS, Albany, CA, USA) as template. The PCR product was cloned into the entry vector pDONR207 using BP clonase II (Life Technologies). The resulting entry clone was used to transfer the fragment into the expression destination vectors pBRACT214m-ZmUBIp and pBRACT214m-HvDMC1p using LR Clonase (Life Technologies) to make ZmUBIp:GUSPlus and *HvDMC1*p:GUSPlus constructs, respectively.

A 900 bp fragment corresponding to the 3′ end of *HvDMC1* coding sequence was PCR amplified using two *HvDMC1* specific primers with Gateway sites (*attB1-HvDMC1* and *attB2-HvDMC1*) and the full-length *HvDMC1* cDNA plasmid as DNA template. The obtained PCR fragment was cloned into the entry vector pDONR207 then transferred into pIPKb007 destination vector (Himmelbach *et al.*, 2007) using Gateway BP and LR Clonase as above (Life Technologies). The final *HvDMC1*^{RNAi} construct therefore had the RNAi cassette under the transcriptional control of maize ubiquitin promoter.

HvDMC1^{RNAi}, ZmUBIp:GUSPlus and HvDMC1p:GUSPlus constructs were transferred into *Agrobacterium tumefaciens* AGL1 strain containing the plasmid helper pSoup. Barley cv. Golden Promise transformation was performed by the Functional Genomics Facility at The James Hutton Institute, Dundee, UK using immature embryos under hygromycin selection as described in Harwood *et al.* (2009). Briefly, 100 immature embryos (1.5–2 mm) were isolated from sterilized seeds and plated on a Petri dish containing callus induction medium until inoculation with overnight culture of *Agrobacterium* clone cultures. Individual embryos were fully covered with *Agrobacterium* culture and transferred to a fresh plate. After 3 d, embryos were transferred onto a new fresh plate containing hygromycin (100 mg l^{-1}) and Timentin (160 mg l^{-1}) and this step repeated every 2 weeks for a total of 6 weeks. The resulting calli were moved to a transition medium in the presence of hygromycin and Timentin for another 2 weeks and the growing shoots were transferred onto rooting medium in glass tubes. Empty vector (EV) was included as control. Rooting T0 transgenic plants were transferred into soil in the glasshouse and grown to maturity.

For *HvDMC1*^{RNAi}, hygromycin-resistant T0 transgenic lines were grown in the glasshouse to maturity. Twenty T1 seeds per line were germinated on solid agar (0.5% phytogel) in the presence of 100 µg ml^{-1} of hygromycin (Jacobsen *et al.*, 2006) to detect the presence of the transgene. Eight to twelve hygromycin-resistant transgenic seedlings were transferred into 6-inch pots of soil and grown in the glasshouse and their vegetative growth and fertility monitored. In the T1 generation, seeds-per-tiller was scored for all transgenic lines including lines that were transformed with empty vector (EV). Untransformed seeds were also germinated on solid agar (0.5% phytogel) without hygromycin.

For GUSPlus lines, T1 seeds were germinated on solid agar (0.5% phytogel) in the presence of 100 µg ml^{-1} of hygromycin (Jacobsen *et al.*, 2006) and resistant seedlings were collected for immediate β-glucuronidase (GUS) histochemical staining. Other seedlings were transferred into soil in the glasshouse and grown to maturity and their mature leaves, roots, stems, and meiotic inflorescences collected for GUS staining. WT barley Golden Promise inflorescences and seedlings were included as negative controls. Freshly collected plant material was fixed in 10 mM MES pH 5.6, 300 mM mannitol, and 0.3% formaldehyde for 45 min at room temperature. The samples were then washed three times in 20 mM sodium phosphate pH 7.0 and 0.2 mM EDTA with an incubation time of 1 min. Washed samples were immersed in GUS staining buffer (50 mM sodium phosphate pH 7, 1 mM EDTA, 0.1 mM potassium ferricyanide, 0.1 mM potassium ferrocyanide, 20% methanol and 1 mM X-GlcA), vacuum

infiltrated for 2 min then incubated at 37 °C for 16 h. The stained material was repeatedly de-stained and stored in 70% ethanol at room temperature.

Cryosection

Fixed GUS stained spikes were used for sectioning with the Cryostat CM1100 (Leica). A thin layer of tissue freezing medium (Jung or TissueTek) was spread on the surface of the specimen holder and left to freeze at −20 °C. Individual spikelets were carefully removed from the rachis using a clean one edge razor blade. One spikelet was mounted on the flat freezing medium surface, covered with more medium, and left to freeze fully. The 20 µm thick sections were captured on the slide then brought to room temperature. Samples were left to air dry before imaging with a light microscope.

Sequence comparison across barley germplasm

Three different published whole genome exome capture datasets were used to investigate natural variation in *HvDMC1* across the barley germplasm. The first dataset with 96 elite spring barley accessions was obtained from Mascher *et al.* (2017) and the remaining two datasets with 129 landraces and 90 wild barley accessions (*Hordeum vulgare* ssp. *spontaneum*), curated to remove nine accessions with dubious provenance, were obtained from Russell *et al.* (2016). The three datasets were analysed independently. Mapping and SNP calling were conducted according to Mascher *et al.* (2017). The unfiltered VCF files were further filtered with the following parameters: only retaining variants which had data for 95% of the samples; at least 98% must be homozygous; they had a minimum average coverage of eight reads; and they had a VCF SNP quality score of over 30. Additionally, heterozygous singletons and all insertions and deletions were removed. Filtering was not carried out against minor alleles given the high number of singleton alleles in wild barley accessions found by Russell *et al.* (2016). All identified variants and their positions are listed in Supplementary Tables S4–S6.

Results

Mapping of the desynaptic mutant des5

Using its severe semi-sterile phenotype as a recessive Mendelian character (Fig. 1A, B), we mapped *des5* to a ~1.7 cM interval between the flanking SNP markers 11_10851 and 11_10174 in the central region of barley chromosome 5H, within the introgression highlighted by the comparison of BW243 and Bowman. The region of the genome delineated by segregation of these marker loci in the F_2 is substantial at 407 Mb and includes the centromeric/peri-centromeric region. Given this location (International Barley Genome Sequencing Consortium *et al.*, 2012) precludes classical fine genetic mapping, a positional candidate gene approach was adopted. The gene content of the region was scrutinized using the recently available sequence of the barley genome (Mascher *et al.*, 2017), which indicated that the region contains 1943 high confidence gene models of which 535 are represented in transcriptome RNA-seq data derived from staged anther tissue at prophase I (M. Schreiber, personal communication). *HvDMC1* was identified as a strong candidate given its known meiotic phenotype (Bishop *et al.*, 1992; Klimyuk and Jones, 1997; Nakashima *et al.*, 2004) and drastic effect on fertility.

DMC1 gene structure and natural variation in barley

BLAST searches against the genome sequence revealed that barley carries a single copy of *HvDMC1* (AF234170) corresponding to the gene model HORVU5Hr1G040730.3 (Mascher *et al.*, 2017) and to the full-length cDNA JQ855497.1 (Barakate *et al.*, 2014). The 5′-end of barley *DMC1* cDNA was determined by rapid amplification of cDNA ends (RACE)-PCR and revealed the presence of a short intron in the 5′-UTR when compared with the previously reported gene annotation (AF234170) (Fig. 1C). The corrected gene model contains 15 exons, including an intron in the 5′ UTR (Fig. 1C; Supplementary Fig. S2) and encodes a protein of 344 amino acids (Fig. 1D; Supplementary Fig. S3). The *DMC1* exon:intron gene structure and the translated protein show very high conservation in other grasses including maize, rice, and wheat (Ding *et al.*, 2001; Devisetty *et al.*, 2010; Etedali *et al.*, 2011) throughout the length of their amino acid sequences (see Supplementary Fig. S3) including the ATP binding domains Walker A/B and ssDNA binding loops 1 and 2 (Fig. 1D). We investigated the genetic variation of HvDMC1 by scrutinizing publicly available barley exome capture data (see Materials and methods). In total 28 SNPs were identified with the majority distributed across the introns and the two UTRs (Fig. 1C triangles; Supplementary Tables S4–S6). Only three SNPs were found in the coding sequence, all of which were singletons found only in *H. v. spontaneum* lines, with two causing synonymous changes (Fig. 1C, green triangles) and one non-synonymous (Q274H, Fig. 1C, red triangle). The potential impact of the non-synonymous SNP at position 274 on the protein was checked using PROVEAN (Choi and Chan, 2015). However, this predicted non-synonymous change (Q274H) did not affect the predicted protein conformation (Supplementary Fig. S4).

HvDMC1 *expression in plant tissue*

The corrected gene model was searched against the RNA-seq data of the barley Morex genome assembly database (International Barley Genome Sequencing Consortium *et al.*, 2012) which contains next-generation sequencing of total RNA extracted from three replicates each of eight different samples (International Barley Genome Sequencing Consortium *et al.*, 2012). We found that *HvDMC1* RNA is observed in all tissues but high in young 5 mm developing inflorescence and highest in 1–1.5 cm inflorescences corresponding to pre-meiosis and meiosis stages respectively (Fig. 2A), which is consistent with previous studies in Arabidopsis (Li *et al.*, 2012). To explore the specificity of the *HvDMC1* promoter, including the 5′-UTR, we used the highly sensitive β-glucuronidase *UidA* reporter gene (GUS). Meiotic inflorescences of wild-type (WT) and T0 transgenic *HvDMC1*p:GUSPlus barley plants and their corresponding hygromycin resistant T1 seedlings were stained for histochemical GUS activity (Fig. 2B–K). Non-transformed plants show no GUS activity in meiotic inflorescence (Fig. 2B) but strong GUS activity was detected in meiotic inflorescences of *HvDMC1*p:GUSPlus plants (Fig. 2C). We found no GUS activity in wild-type plants nor in T1 seedlings of the *HvDMC1*p:GUSPlus lines (Fig. 2D). As a positive control, hygromycin-resistant T1 seedlings of transgenic lines where GUS is under the control of the constitutive maize ubiquitin promoter (ZmUBIp) showed strong GUS activity throughout all plants tissue (Fig. 2E). We observed no GUS staining

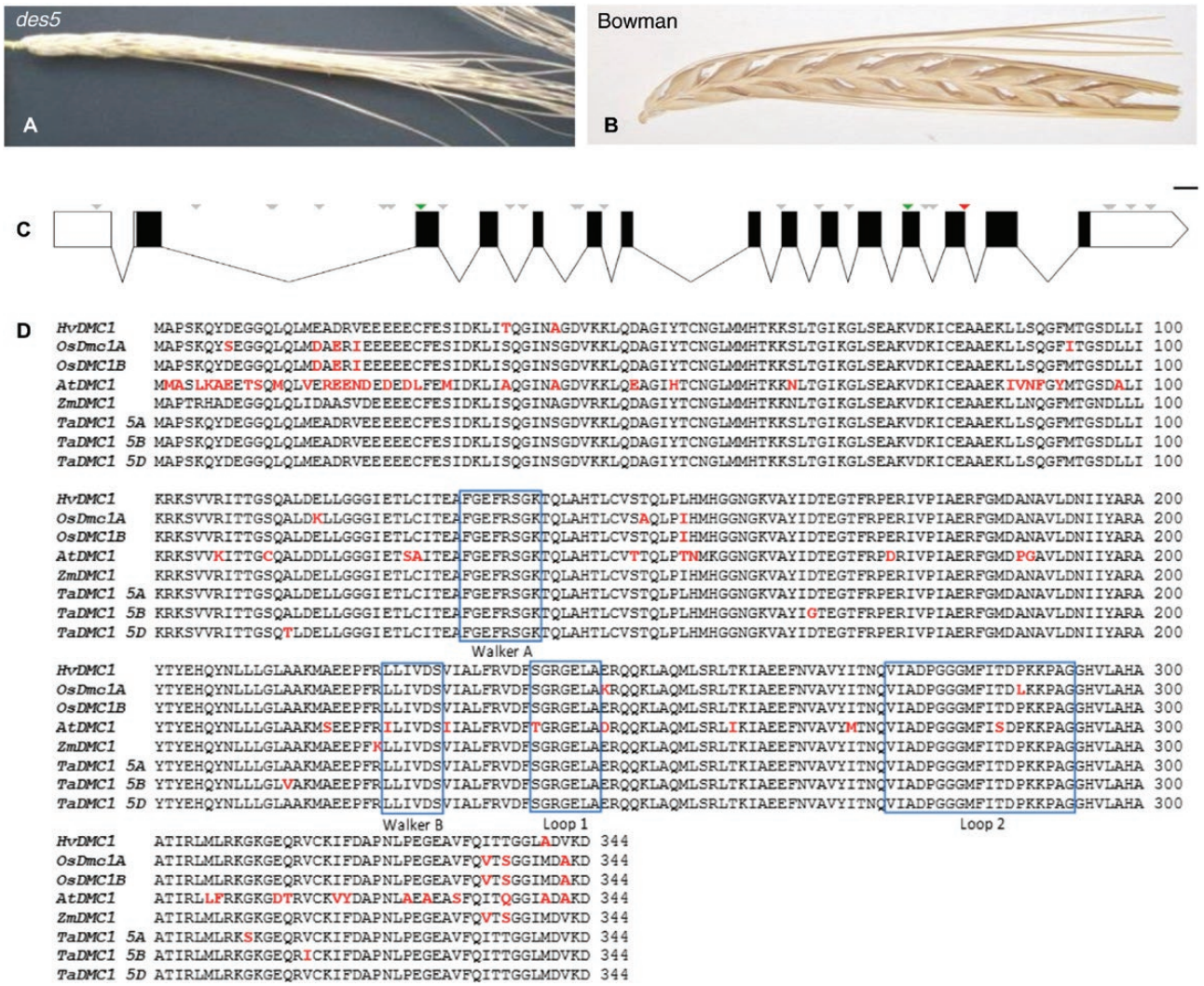

Fig. 1. Fertility in *des5* mutant and structure of the *HvDMC1* gene. (A, B) The near-isogenic line BW243(*des5*) (A) shows low levels of fertility with an average of 1.2±0.9 seed per plant compared with cv. Bowman wild-type (B). (C) Cartoon of the gene structure of HORVU5Hr1G040730.3, which encodes *HvDMC1* in barley, showing the position of the 31 identified SNPs in intron or UTR regions as grey arrows. The two SNPs causing synonymous changes in the coding sequence are marked with green arrows and the SNP causing the non-synonymous change is marked with a red arrow. Scale bar represents 100 bp. (D) Alignment of barley (*Hordeum vulgare*; Hv), rice (*Oryza sativa*; Os), maize (*Zea mays*; Zm), bread wheat (*Triticum aestivum*; Ta), and Arabidopsis HvDMC1 amino acid sequences showing the conserved ATP binding domains Walker A and B motifs and ssDNA binding loops 1 and 2 in transparent boxes. Amino acids in red indicate non-identity between orthologous sequences.

in the roots (Fig. 2F) and leaves (Fig. 2G) of wild-type plants or transgenic lines under *HvDMC1* promoter control. On the other hand, male (Fig. 2H–I) and female (Fig. 2J) reproductive tissues were highly stained. These results indicate that DMC1p:GUSPlus expression appears to be inflorescence specific, although anther sectioning shows that it is not exclusive to meiotic tissue (Fig. 2K).

HvDMC1^{RNAi} *have highly reduced chiasmata*

We used RNA interference to specifically knockdown DMC1 in wild-type barley (cv. Golden Promise) plants. We generated 30 *HvDMC1*^{RNAi} lines, selecting multiple shoots from 16 initial immature embryos. Four of the *HvDMC1*^{RNAi} lines from independent immature embryos showed low to very low fertility at T0 (see Supplementary Fig. S5A) and further semi-sterile lines were detected in the subsequent generation. We selected two *HvDMC1*^{RNAi} lines (11-2-2 and 16-3-1) to carry out cytological analysis and compare with their wild-type background Golden Promise (Fig. 3; Supplementary Figs S5, S6). Line *HvDMC1*^{RNAi}16-3-1 plants were sterile (Fig. 3A) compared with Golden Promise plants (Fig. 3B) grown under the same conditions. This line had an average of 0.78±1 chiasma per cell (n=23) (Supplementary Fig. S5B) and mostly exhibited univalents (Fig. 3C–D; Supplementary Fig. S5B–C), with cells occasionally showing up to five chiasmata (Supplementary Fig. S5B). In Golden Promise, we found an average of 16.13±1.25 chiasmata per cell (n=8) with only ring bivalents formed (Fig. 3E–F; Supplementary Fig. S5B–C). The second line, *HvDMC1*^{RNAi}11-2-2, showed an inconsistent phenotype with both somewhat normal and abnormal metaphases (Supplementary Fig. S6) but similar to *des5*. The absence of COs in these transgenic lines is consistent with that of previously characterized DMC1 mutants.

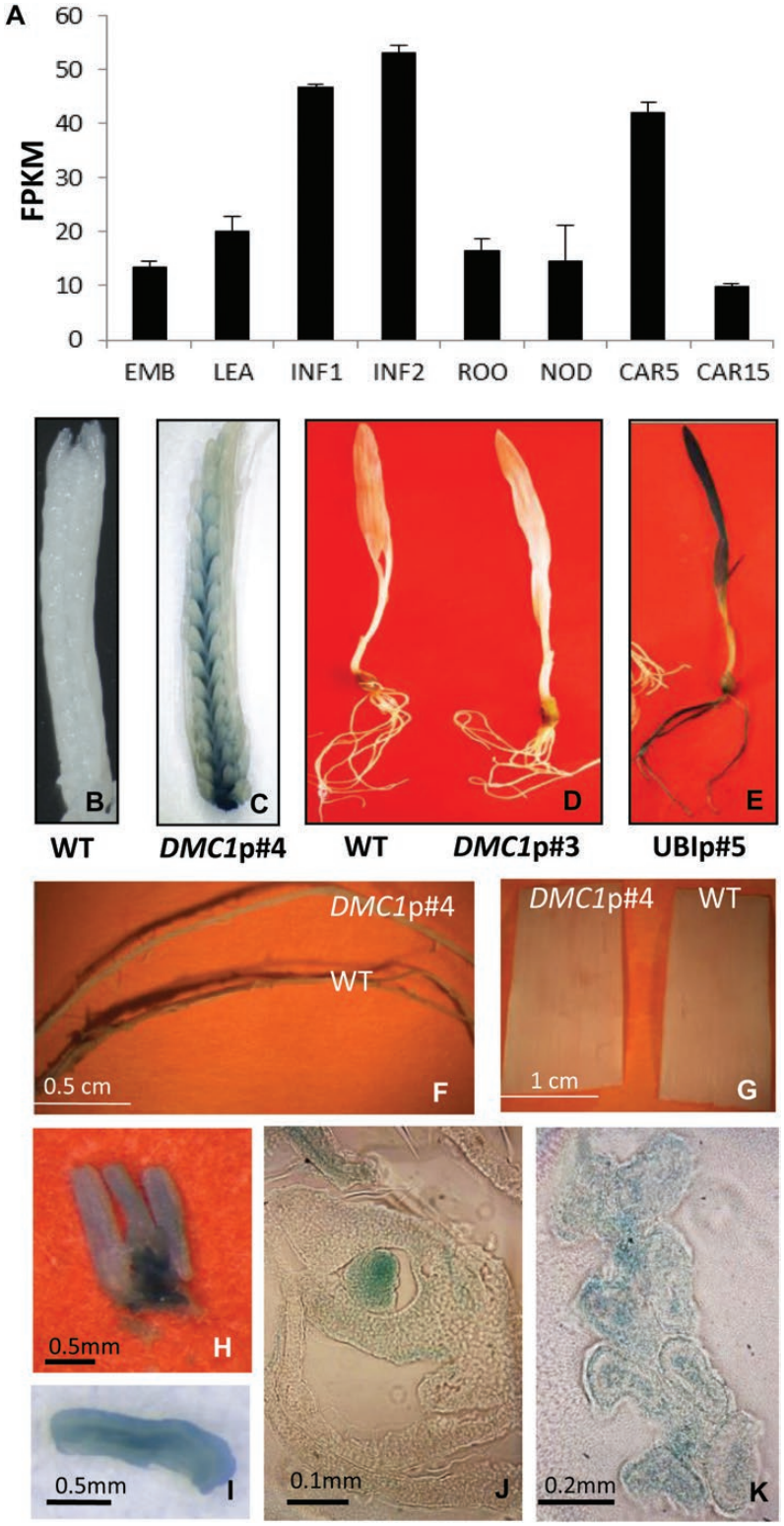

Fig. 2. *HvDMC1* expression. (A) The graph shows *HvDMC1* expression levels in different organs of barley cv. Morex using RNA-seq data. Error bars represent the SD (n=3). CAR5, developing grain, bracts removed (5 d post-anthesis); CAR15, developing grain, bracts removed (15 d post-anthesis); EMB, 4-day-old embryos dissected from germinating grains; FPKM, fragments per kb of transcript per million mapped reads; INF1, young developing inflorescences (5 mm); INF2, developing inflorescences (1–1.5 cm); LEA, shoots from seedlings (10 cm shoot stage); NOD, developing tillers at the six-leaf stage, third internode; ROO, roots from seedlings (10 cm shoot stage). (B–K) Histochemical analysis of *HvDMC1*p:GUSPlus transgene expression. Plant material was stained with X-glcA to detect GUS activity. (B, C) Spikes of wild-type (WT) (B) and *HvDMC1*p:GUS transgenic line 4 (*HvDMC1*p#4) (C). (D) seedlings of WT and *HvDMC1*p#4. (E) seedlings of *ZmUBI*p:GUS line 5 (UBIp#5) used as positive control. (F, G) Roots (F) and leaves (G) of WT and *HvDMC1*p#4. (H, I) Isolated anthers of *HvDMC1*p#4. (J) Cross section of *HvDMC1*p#4 floret showing high GUS staining of ovary. (K) Cross section of *HvDMC1*p#4 anthers showing GUS activity in most of the anther tissues.

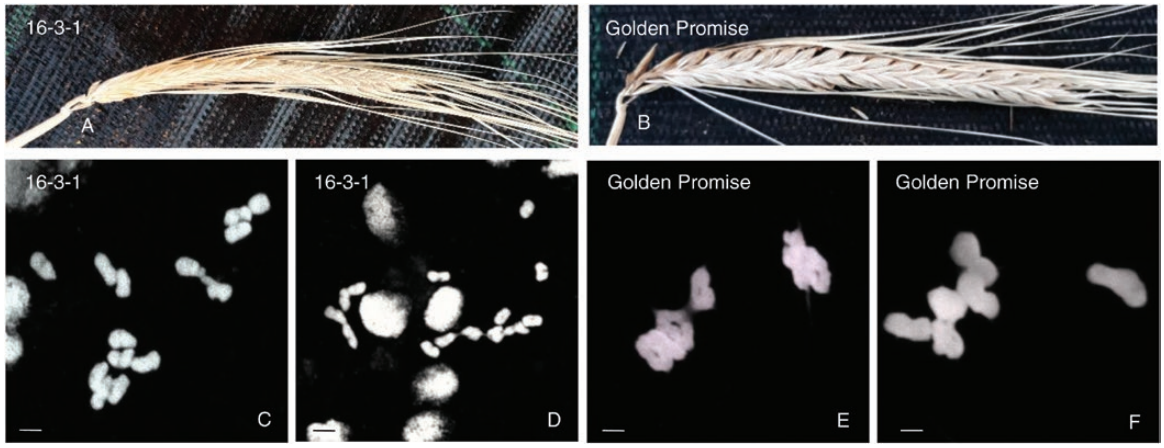

Fig. 3. Chromosome behaviour in *HvDMC1*^{RNAi} 16-3-1 and Golden Promise. (A, B) *HvDMC1*^{RNAi}16-3-1 (A) is semi-sterile compared with wild-type Golden Promise plants grown under the same conditions (B). (C–F) Metaphase spreads of *HvDMC1*^{RNAi}16-3-1 (C, D) exhibit multiple univalents compared with metaphase spreads of Golden Promise plants (E, F), which exhibit seven ring bivalents. Scale bar 5 μm.

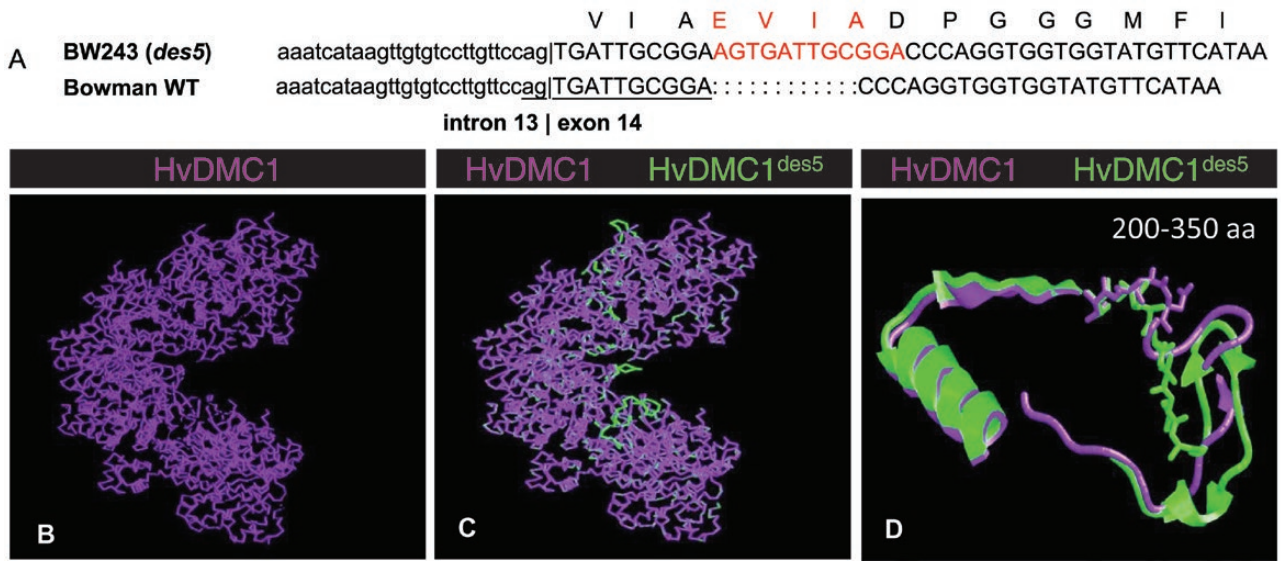

Fig. 4. HvDMC1 is mutated in *des5* (BW243). (A) Details of the 12 bp duplication (in red) that causes the insertion in *des5* cds in exon 14. The protein model for HvDMC1 in wild-type was obtained by submitting the sequence to swissprot. (C) The Swiss-Prot protein model for HvDMC1^{des5} (green) shows some significant differences compared with the wild-type (magenta) when aligning. (D) The model of the protein region from amino acid 200 to 350 shows the structure difference caused by the duplication of four amino acid motifs in *des5* (green) compared with the wild-type (magenta).

des5 *carries a mutation in* HvDMC1

Sequencing the coding domain of *HvDMC1* in BW243, Bowman and the original background cv. Betzes (see Supplementary Tables S1, S2) indicated that *HvDMC1* in BW243 contains an insertion that appears to have resulted from a 12 bp duplication that includes the boundary between intron 13 and exon 14 (Fig. 4A), confirmed by cDNA sequencing (Supplementary Fig. S7). Duplication in *des5* maintains the reading frame but introduces four amino acids, EVIA, into exon 14 between positions 276 and 277 (Fig. 4A) that would potentially disrupt the loop 2 domain of the protein that is postulated to be involved in DNA binding (Kinebuchi *et al.*, 2004). SWISS-MODEL (Arnold *et al.*, 2006) indicated that the HvDMC1 3D protein formed an L-shape structure (Fig. 4B), as previously predicted (Kinebuchi *et al.*, 2004; Du and Luo, 2013). Similarly, the DMC1^{des5} protein model also predicts an L-shape structure but has a slightly different 3D conformation when superposed onto the wild-type protein (Fig. 4C). The modelling indicated that the majority of the DMC1 protein in *des5* is unchanged except for the region between the 200th and 350th amino acid (Fig.4D), which could affect protein stability and/or polymerization of the nucleofilament (Du and Luo, 2013).

des5 *displays abnormal meiosis*

We performed DNA *in situ* hybridization with telomere and centromere probes on isolated meiocytes to monitor the onset of meiosis in *des5* (see Supplementary Fig. S8). We found that *des5* telomeres clustered to one side of the nucleus (Supplementary Fig. S8) as previously reported in barley and other grasses (Carlton and Cande, 2002; Mikhailova *et al.*, 2006; Colas *et al.*, 2008; Phillips *et al.*, 2012). A similar phenotype is shown by *dmc1* mutants in rice (Wang *et al.*, 2016)

and mouse although the latter also had a possible persistent telomere clustering (Liebe *et al*., 2006). We also found that centromeres paired at the opposite side in both wild-type and *des5* (Supplementary Fig. S8), as previously described for early meiotic events in *dmc1* mutants (Deng and Wang, 2007; Da Ines *et al*., 2012) although in one of the rice mutants, it was also found that the centromere pairing dynamics differed at later stages. DAPI staining images of early prophase I (leptotene and zygotene stages) look similar for Bowman (Fig. 5A–B and *des5* (Fig. 5D, E). At pachytene stage (Fig. 5C, F), areas of unpaired chromosomes are visible in *des5* (Fig. 5F, arrows), similar to that previously reported in rice (Deng and Wang, 2007, Wang *et al*., 2016). At metaphase I, wild-type barley showed seven ring bivalents (Fig. 5G) corresponding to >14 chiasmata/cell, as previously reported (Colas *et al*., 2016), and the chromosomes separated regularly and equally during anaphase I (Fig. 5H). In *des5*, metaphases were hard to find due to premature senescence of the anthers but when present, the chromosomes appeared thicker and stickier than in wild-type and were found either as unpaired univalents (Fig. 5J) or rod bivalents

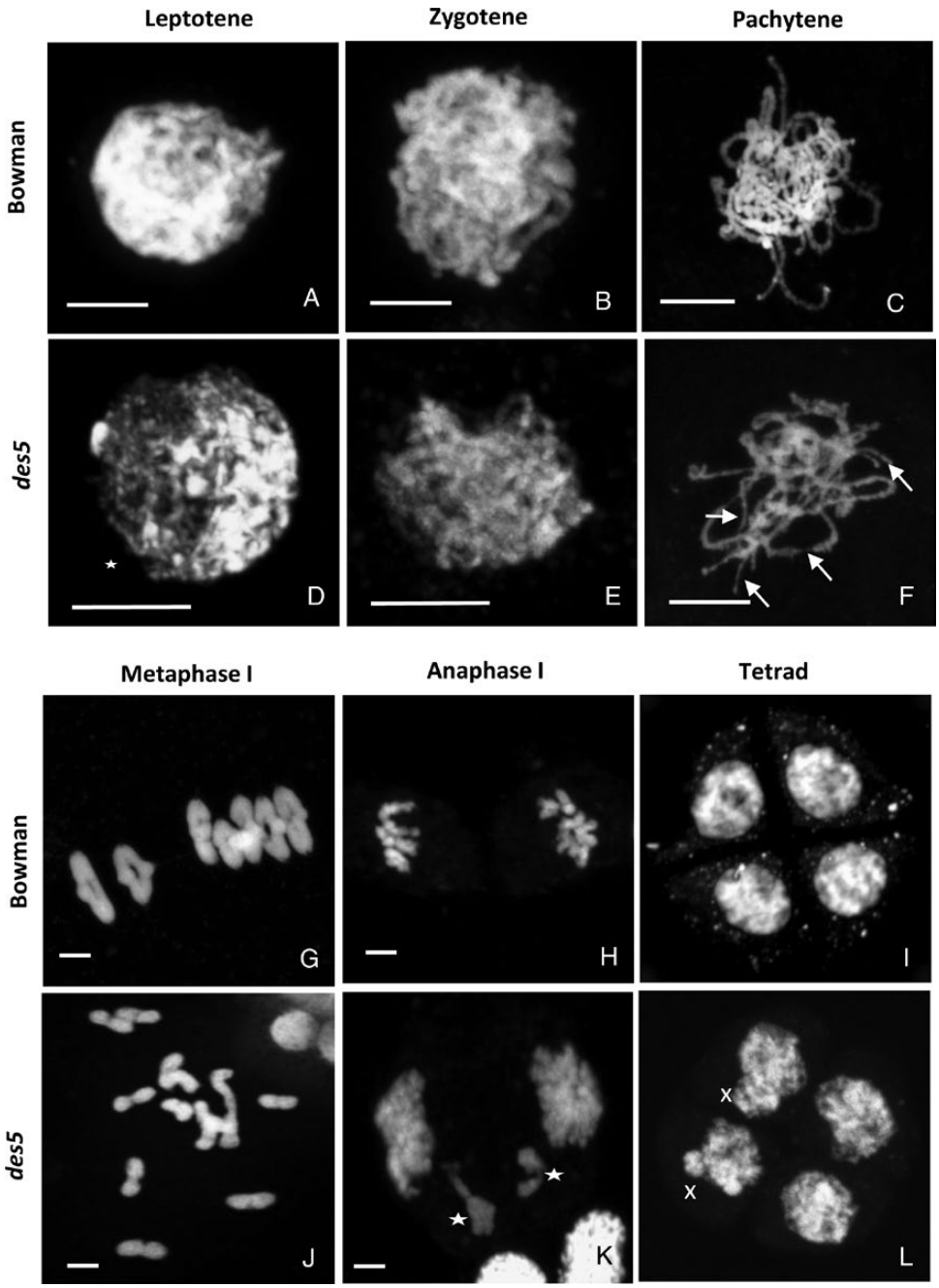

Fig. 5. Abnormal meiotic behaviour in *des5*. (A–F) Nuclei from wild-type Bowman at leptotene (A), zygotene (B), and pachytene (C) stages were compared with nuclei from *des5* at leptotene (D), zygotene (E), and pachytene (F) stages. There is no obvious difference between Bowman and *des5* at leptotene and zygotene stage, but at the pachytene stage, *des5* shows unpaired regions (arrows). (G–L) Bowman exhibits seven ring bivalents at metaphase I (G), normal anaphase I (H) and tetrads (I) but *des5* shows univalents at metaphase I (J), lagging chromosome at anaphase I (stars) (K) and unbalanced tetrads (crosses) (L). Scale bar represents 5 μm.

(Supplementary Fig. S9A). *des5* exhibited 4.18±2.79 chiasmata per cell (n=28) with a range of 1–9 and various numbers of ring and rod bivalents (Supplementary Fig. S9B–C). Lagging chromosomes were observed in *des5* (Fig. 5K, white star) leading to unbalanced tetrads when formed (Fig. 5L, white cross).

des5 *has compromised synapsis*

To investigate when meiosis was perturbed, we used immunocytology with antibodies against TaASY1 and HvZYP1 to follow the progression of synapsis in wild-type and *des5* (Fig. 6; Supplementary Figs S10, S11). In wild-type, homologous chromosomes were progressively linked to one another via the protein ZYP1 (magenta) starting from leptotene (Fig. 6A) and synapsed during zygotene (Fig. 6B). At pachytene, chromosomes are fully synapsed with a continuous ZYP1 labelling (Fig. 6C) as previously described (Phillips *et al.*, 2012; Colas *et al.* 2016). In *des5*, ASY1 axes (green) formed during leptotene and ZYP1 did polymerize during zygotene (Fig. 6D–F), potentially initiating

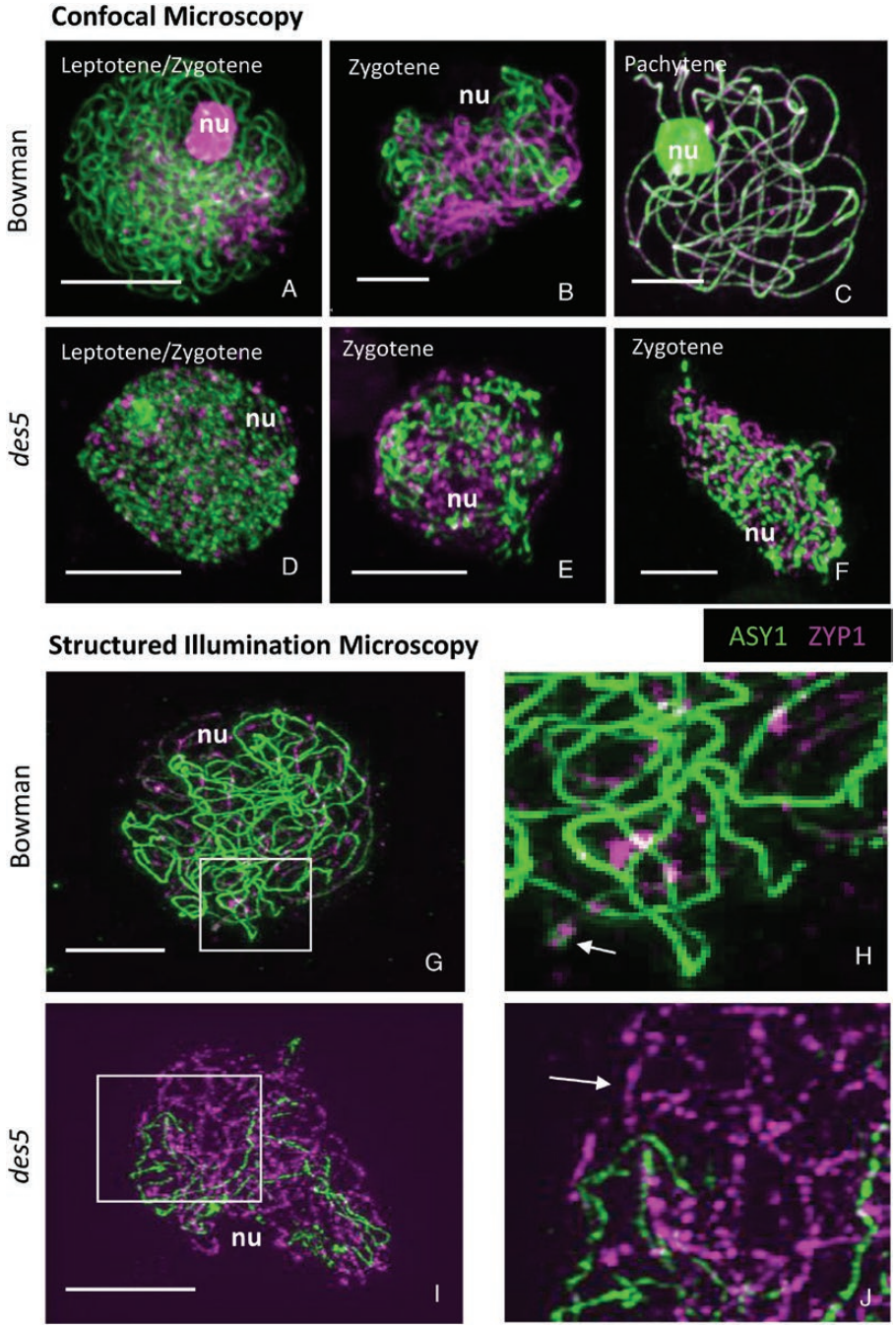

Fig. 6. Analysis of synapsis. (A–C) In Bowman, synapsis, monitored by anti-HvZYP1 (magenta), starts from the telomeres (A); during the zygotene stage HvZYP1 polymerizes between the homologous chromosomal axes (labelled by anti-TaASY1, green) (B); and synapsis is complete at pachytene with both ASY1 and ZYP1 overlapping (C). (D–F) In *des5*, synapsis seems to start normally (D), but the polymerization of HvZYP1 appears to be compromised (E, F). (G, H) 3D-SIM in Bowman shows normal synapsis (G), with the tripartite structure typical of paired chromosomes (arrow) already visible from zygotene (H). (I, J) In *des5* although HvZYP1 (magenta) polymerizes (I), the tripartite structure is not visible (arrow) (J). nu, the nucleolus. Scale bar represents 5 μm.

synapsis between the homologous chromosomes. However, although chromatin staining suggested that the cells were at pachytene (see Supplementary Fig. S10), we were unable to find any cells with full polymerization of ZYP1 (continuous ZYP1 signal) and full synapsis (pachytene stage definition) but instead found an excess of cells that appeared to be at a zygotene-like stage (Fig. 6F). Absence of synapsis or abnormal synapsis (dots and stretches) have been previously described in *dmc1* mutants (Klimyuk and Jones, 1997; Deng and Wang, 2007; Wang *et al.*, 2016). When checking synapsis using 3D-SIM (Fig. 6B; Supplementary Fig. S10), which gives a 100–120 nm resolution, we could see homologous chromosomes (green) paired via ZYP1 (magenta) during mid-zygotene (Fig. 6G, H arrow) in the wild-type but not in *des5* (Fig. 6I, J arrow). In addition, the diameter of wild-type and *des5* nuclei was measured using DAPI fluorescence, which indicated that that while wild-type showed increased size of nuclei during synapsis, the size of the *des5* nuclei did not expand to a similar extent (Supplementary Fig. S12).

DMC1 behaviour in barley

It has been shown that recombination proteins such as RAD51 start loading onto the chromosomal axes near the telomeres in barley (Higgins *et al.*, 2012; Colas *et al.*, 2016) but the behaviour of DMC1 in early meiosis in barley has not been reported. Using custom antibodies against HvDMC1 (green) and TaASY1 (magenta) in Bowman and *des5*, we found a similar pattern to that of RAD51, with DMC1 loading as a cluster (multiple foci) at one side of the nucleus at leptotene (Fig. 7A–C; Supplementary Fig. S13A) and loading onto the chromosome axis during zygotene (Fig. 7D–F; Supplementary Fig. S13A). The number of DMC1 foci increases in the nucleus from leptotene (142.9±35.1) to zygotene (312.5±82.8) (see Supplementary Fig. S13B, C). In *des5,* foci could be detected as a cluster on one side of the nucleus (Fig. 7G–L; Supplementary Fig. S13A) as in the wild-type, but the clusters were smaller (Fig. 7G–L; Supplementary Fig. S13A). At zygotene we still see green foci in *des5*, but they are mainly located in the cytoplasm (Supplementary Fig. S13) which may indicate a problem with

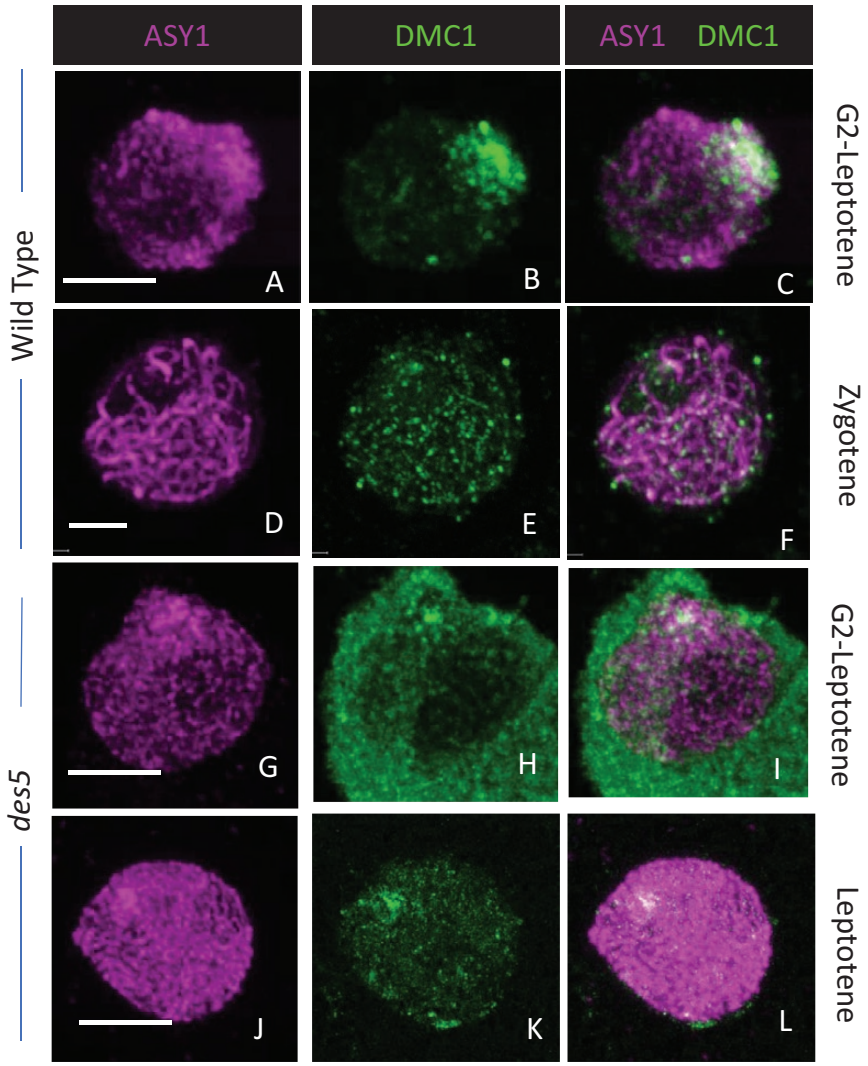

Fig. 7. HvDMC1 labelling in early meiosis. ASY1 (magenta) and DMC1 (green) behaviour in Bowman (A–F) and *des5* (G–L). (A–C) HvDMC1 starts loading at one side of the nucleus. (D–F) The number of foci increases and appear throughout the nucleus during zygotene as well as on ASY1 axes. (G–L) In *des5*, HvDMC1 also starts loading at one side of the nucleus, but with a very limited signal compared with Bowman lines. Scale bar represents 5 μm.

the functionality of the protein or that the antibody forms unspecific poly-complexes in the absence of a stable protein.

des5 *shows a semi dominant recombination phenotype*

To explore whether *des5* had any effect on recombination, we constructed genetic maps from the F_2 populations of crosses between BW243(*des5*) × cv. Barke and BW243(*des5*) × cv. Morex. The maps derived from the two F_2 mapping populations were then compared with a reference SNP map constructed from a recombinant inbred line (RIL) population derived from a cross between cv. Morex × cv. Barke, taking into account the different recombination frequencies expected of the two population types (Comadran *et al.*, 2012) (Fig. 8; Supplementary Fig. S14A–F). Genetic maps from the crosses involving *des5* were generally shorter than expected. The comparison of total genetic map lengths derived from shared SNP loci between the *des5* F_2 populations (618.0 and 575.2 cM) and the respective portions of the reference mapping population (734.0 and 767.8 cM) (two-tailed *t*-tests on underlying recombination frequencies $P<1.0\times10^{-4}$) corresponded to two fewer COs per cell in the *des5* heterozygotes than expected (11.9 and 11.7 versus 13.8 and 14.2) within the intervals bounded by the common marker loci. This reduction was particularly evident in the central peri-centromeric regions of the chromosomes as shown by a comparison of chromosome 3H (Fig. 8) where the central 40.9 cM on the cv. Morex × cv. Barke RIL map (Comadran *et al.*, 2012) (11_10672 to 11_20659) is reduced to 16.5 cM in the BW243(*des5*) × cv. Barke and 17.9 cM in the BW243(*des5*) × cv. Morex F_2 populations. This reduction in recombination was less evident in other chromosomes such as 7H but this did exhibit a change in recombination distribution with loci 26 cM apart in the short arm in the standard map being unlinked in the F_2 populations derived from BW243(*des5*) (see Supplementary Fig. S14).

Discussion

The meiotic recombination protein DMC1 has been extensively studied in model systems, demonstrating a conserved role in meiosis across eukaryotes (Bishop *et al.*, 1992, Habu *et al.*, 1996; Doutriaux *et al.*, 1998; Kathiresan *et al.*, 2002). There have been a number of *in silico* studies of DMC1 in grass species, such as barley, wheat, and maize (Shimazu *et al.*, 2001; Mikhailova *et al.*, 2006; Devisetty *et al.*, 2010; Etedali *et al.*, 2011; Barakate *et al.*, 2014), but they did not provide functional analysis to confirm DMC1's role in a large genome crop.

We found that barley carries a single copy *HvDMC1* (AF234170; HORVU5Hr1G040730.3; JQ855497.1) and we confirmed the gene structure by RACE-PCR (Fig. 1C; Supplementary Fig. S2), revealing the presence of a short intron in the 5′-UTR when compared with the previously reported gene annotation (AF234170) (Barakate *et al.*, 2014, Mascher *et al.*, 2017). Analysis of a large sample of *Hordeum vulgare* accessions (Russell *et al.*, 2016) showed a near total absence of non-synonymous variation, which concords well with the conservation of the coding sequence within the Triticeae and beyond (Fig. 1D; Supplementary Fig. S3) (Petersen and Seberg, 2002; Lin *et al.*, 2006). A single non-synonymous SNP was found (Q to H change at position 274 (Fig. 1C, red arrow; Supplementary Fig. S4) within a single *Hordeum vulgare* ssp *spontaneum* accession (FT64) from Israel. This polymorphism is within a highly conserved region directly before the loop 2 domain and appears to be unique, as it is not found in any of the DMC1 sequences of related Triticeae species (Petersen and Seberg, 2002; Petersen *et al.*, 2006; Sha *et al.*, 2010; Sun and Zhang, 2011). The functional significance of this SNP is unclear, although it is possible that a mildly deleterious allele could be maintained given the reduced selection efficiency in the recombination-poor pericentromeric regions (International Barley Genome Sequencing Consortium *et al.*, 2012; Baker *et al.*, 2014; Mascher *et al.*, 2017) and the maintenance of potentially functional DMC1 variants in other species (Stolk *et al.*, 2012).

Expression surveys indicate that the *HvDMC1* transcript is detected at a low level in all tissues surveyed but at much higher levels in meiotic tissues (Fig. 2). The histochemical GUS staining of *HvDMC1*p:GUSPlus transgenics similarly revealed strong expression in meiotic inflorescences but failed to detect GUS activity in seedlings as previously reported in Arabidopsis (Li *et al.*, 2012). In a parallel study using GFP as a reporter for HvDMC1 promoter activity, expression throughout the inflorescence was also observed (our unpublished results).

In mammals, DMC1 mutants generally have defective synapsis with premature arrest during meiosis prophase I leading to sterility (Pittman *et al.*, 1998; Yoshida *et al.*, 1998; Keeney *et al.*, 2007). However, in Arabidopsis and rice, although plants are severely affected in their fertility with univalents apparent at metaphase I, they are not completely sterile as a sufficient number of pollen mother cells reach maturity due to random chromosome segregation (Couteau *et al.*, 1999; Da Ines *et al.*, 2013). Similarly, in barley, the *HvDMC1*^{RNAi} lines showed low to very low levels of fertility in the T1 generation (Fig. 3; Supplementary Fig. S5) with lines *HvDMC1*^{RNAi}11.2 and *HvDMC1*^{RNAi}16.3 in particular producing an average of 7.7±4.5 and 6.9±5.6 seeds per plant respectively compared with 21.9 seeds in empty vector (EV) transformants. These *HvDMC1*^{RNAi} lines also exhibited disturbed metaphase I phenotypes with limited chiasmata resulting in the prevalence of univalents, a phenotype symptomatic of the strong downregulation of DMC1 (Fig. 3; Supplementary Figs S5, S6).

Traditional fine genetic mapping was not possible as a means to identify *des5* given its location in the peri-centromeric region of 5H (International Barley Genome Sequencing Consortium *et al.*, 2012). However a candidate gene approach successfully identified *HvDMC1* within the genomic regions delineated by both F_2 mapping and the near-isogenic line BW243. Sequencing *HvDMC1* genomic DNA and cDNA from anther tissue indicated that BW243(*des5*) had a 12 bp duplication in the coding domain (Fig. 4A; Supplementary Fig. S7). This duplication affects the counterpart of the loop 2 domain of RecA, which is a structurally disordered region that has been shown to be involved in DNA binding in RecA and its eukaryotic orthologs (Voloshin *et al.*, 1996; Bannister *et al.*, 2007; Zhang *et al.*, 2009; Fig. 4B–D).

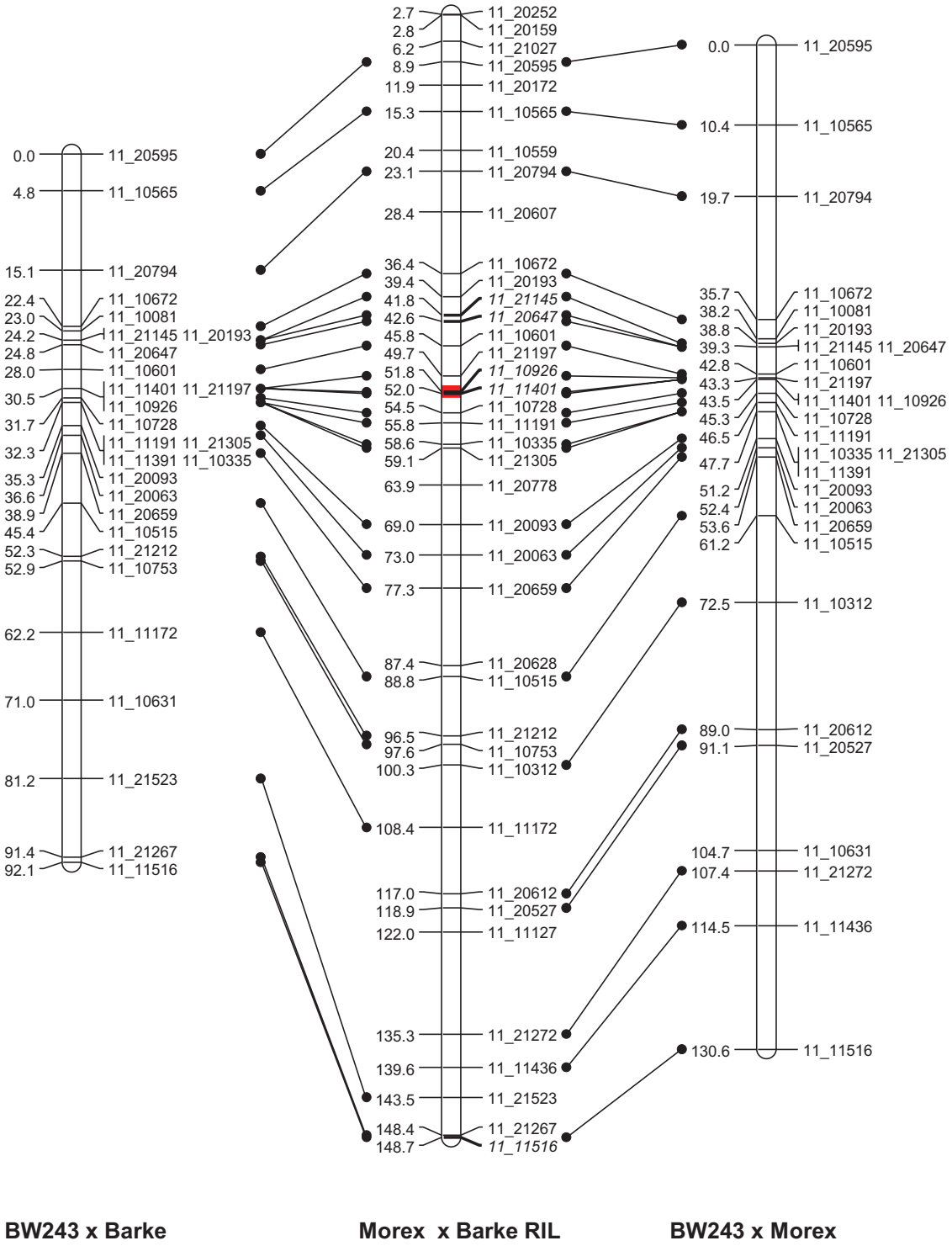

Fig. 8. F_2 genetic maps in *des5* crosses. Comparison of genetic maps for chromosome 3H between the consensus map (derived from Morex × Barke RILs) and those derived from the F_2 populations from the crosses BW243(*des5*) × Barke and BW243(*des5*) × Morex. The centromeric region is marked in red on the RIL map and the position of five unmapped SNPs (in italics) is placed on the RIL map by comparison with other genetic maps (Close *et al.*, 2009) and the physical map (Mascher *et al.*, 2017).

The loop 2 region is located within the centre of the ring of the DMC1 proteins that form the likely catalytic site for the search and exchange of DNA strands (Kinebuchi *et al.*, 2004) within the helical DMC1 filament necessary to assist strand exchanges (Sheridan *et al.*, 2008). It is plausible therefore that the 12 bp duplication present in the *des5* mutant would potentially perturb the binding of DNA and the ability to catalyse strand invasion through the disruption of the structure of the catalytic site. The limited number of chromosomal DMC1 foci in *des5* indicates that the mutation, although severely compromising DMC1 protein, may not be a complete knockout.

DNA *in situ* hybridization indicated that in *des5*, centromere pairing and telomere clustering were unaffected at the onset of meiosis (see Supplementary Fig. S8). This is congruent with

previous analysis in Arabidopsis and rice (Deng and Wang, 2007; Da Ines *et al.*, 2012). We noticed the predominance of early meiotic stages in all our spreads as well as defective synapsis, which could suggest that, as previously reported for *dmc1* mutants, the progression of the meiotic programme is compromised. In mouse, persistent telomere clustering was observed (Liebe *et al.*, 2006), while in rice telomere and centromere pairing dynamics were affected at later stages of meiosis (Deng *et al.*, 2007). The normal early meiotic phenotype could suggest that homologous chromosome searching is not affected, and that pairing could be normal as reported with the rice *OsDMC1a–OsDMC1b* double mutant that exhibits normal chromosome pairing but defective synapsis (Wang *et al.*, 2016), but further study would be needed to confirm this.

The initiation of synapsis seems correct in *des5*, but meiotic cells do not complete synapsis (Figs 5, 6), which corresponds with observations from other species (Habu *et al.*, 1996; Doutriaux *et al.*, 1998; Ding *et al.*, 2001; Deng and Wang, 2007) where mutant cells are arrested at pachytene, before entering apoptosis. Moreover, high resolution microscopy (Fig. 6; Supplementary Fig. S11), indicated that the classical tripartite synaptonemal complex structure was not visible in *des5*, which may suggest abnormal compaction/extension of the chromosome as seen in previous studies in barley mutants with abnormal synapsis (Barakate *et al.*, 2014; Colas *et al.*, 2016, 2017). Given the lack of a pachytene checkpoint in plants (Li *et al.*, 2009), meiosis did progress in *des5* plants but the presence of rod bivalents, and in particular univalents, suggests a major defect in CO formation, including loss of obligate COs (Jones and Franklin, 2006). The subsequent lagging chromosomes would result in unbalanced segregation in daughter cells and their corresponding gametes consistent with the observed problems of fertility. That impaired DMC1 function is the cause of *des5* is supported by the similar phenotype of *HvDMC1*$^{R.NAi}$ knockdown plants. Finally, *des5* labelling with DMC1 antibody has shown that although the antibody seems to behave as in the wild-type (Fig. 7), we observed a faint signal in the nucleus (potentially on the chromatin) that could be caused by polycomplexes formed by the antibody in the absence of a proper protein. The expression of a non-functional or severely compromised DMC1 protein encoded by the *des5* allele could potentially explain the small dominant negative effect observed on recombination in the heterozygote (see Supplementary Fig. S8). The comparison of genetic maps derived from F_2 populations resulting from crosses between BW243(*des5*) and cv. Barke or cv. Morex with the reference genetic map derived from a Morex × Barke RIL population indicated that the F_1 individuals with *des5* present in the heterozgous state showed significantly less recombination. This slight effect on recombination frequency did not affect the fertility of the heterozygous plants. However, the slight semi-dominant effect on recombination observed in the genetic mapping in this study is supported by the reported reduction in CO numbers with up to three rod bivalents per cell observed in F_1 crosses (Hernandes-Soriano, 1973). It is tempting to postulate that the presence of a functionally compromised DMC1 protein encoded by *des5* could interfere with the formation of a fully functional DMC1 protein complex in the heterozygote, with the HvDMC1^{des5} protein incorporated into the helical DMC1 polymeric filament that assists DNA strand exchange (Sheridan *et al.*, 2008). Interestingly the mutation in *des5* shows some analogy to the non-knockout mutant *Dmc1*^{Mei11} in mouse (Supplementary Fig. S15) that is caused by a non-synonymous change within the loop 2 domain and which also shows dominance with defective synapsis, a lack of recombination and sterility in male mice (Bannister *et al.*, 2007). However as *in vitro* competition assays using wild-type and DMC^{Mei11} failed to reveal inhibition of D-loop activity, the explanation of the dominance relationship of the *dmc1*^{Mei11} allele in mouse and *des5* in barley in terms of protein structure remains hypothetical (Bannister *et al.*, 2007).

The cytological characterization of *des5* indicates a conserved role for DMC1 in barley that largely conforms to the phenotype found in model systems. Thus, early meiosis is unaffected with potentially normal homologous chromosome pairing but subsequent synapsis is defective. The presence of univalents at metaphase I suggested a major defect in CO formation, including that of obligate COs (Jones and Franklin, 2006), which led to subsequent problems of unbalanced segregation and ultimately severe problems of fertility. Some aspects of the *des5* phenotype were potentially due to the presence of a non-functional DMC1^{des5} protein. This includes the semi-dominance observed as reduced recombination in the heterozygote, which has parallels with the mouse mutant *dmc1*^{Mei11}.

Overall the phenotype of *des5* is closer to that of the rice double *Tos17* insertion DMC1 mutant (Wang *et al.*, 2016) than that of knockdown OsDMC1–RNAi lines (Deng and Wang, 2007) indicating a conserved role of DMC1 across the grasses. The specificity of phenotypes to specific mutants can make cross species comparisons difficult (Wang *et al.*, 2010; Barakate *et al.*, 2014) but potentially provides additional functional information. Thus the use of *des5* to characterize the role of DMC1 follows the recent positional cloning of another barley desynaptic mutant, *des10*, which enabled dissection of the role of HvMLH3 in barley (Colas *et al.*, 2016). In both cases the particular form of the spontaneous mutant alleles resulted in the coding sequence being maintained in frame, allowing immunolocalization of the protein in both wild-type and mutant, providing novel insights into the importance of the underlying genes in the very early stages of meiosis in this large genome cereal.

In conclusion we identified *desynapsis5* as carrying a mutation in the meiotic gene *HvDMC1* in barley and provide information on the limited natural variation in the species. We identified a 12 bp insertion in *HvDMC1* in *des5* that leads to abnormal synapsis and subsequent chromosome mis-segregation. *HvDMC1* transcript was mainly observed in reproductive tissues, and promoter expression studies showed strong inflorescence specificity. The meiotic phenotype of *des5* is severe and completely congruent with expectations from model species, indicating a conserved role of DMC1 in large genome cereals. The specific nature of the mutation showed similarities to mouse *Dmc1*^{Mei11} and highlights the informativeness of deleterious but non-knockout mutations for the dissection of gene function.

Supplementary data

Supplementary data are available at *JXB* online.

Fig. S1. Initial mapping of *des5*.

Fig. S2. Revised barley *HvDMC1* sequence.

Fig. S3. *HvDMC1* conservation in plants.

Fig. S4. 3D model comparison for *HvDMC1* variant.

Fig. S5. Semi-sterility of *HvDMC1*^{RNAi} transgenics and quantitative analysis of bivalent type.

Fig. S6. *HvDMC1*^{RNAi} *11-2-2* phenotype.

Fig. S7. *HvDMC1*^{des5}cDNA and polymorphism.

Fig. S8. Telomere bouquet in wild-type and *des5*.

Fig. S9. Chiasmata count and quantitative analysis of bivalent type in *des5*.

Fig. S10. Confocal analysis of synapsis.

Fig. S11. Structured illumination microscopy analysis of synapsis.

Fig. S12. Nuclei size in wild-type and *des5*.

Fig. S13. *HvDMC1* behaviour in wild-type and *des5*.

Fig. S14. Comparison of maps derived from F_2 populations derived from BW243 × Morex and BW243 × Barke with Morex × Barke RIL map.

Fig. S15. Barley HvDMC1^{des5} and mouse DMC1^{Mei11} comparison.

Table S1. List of primers used for *HvDMC1* genomic sequencing.

Table S2. List of primers used for *HvDMC1* cDNA sequencing.

Table S3. List of oligonucleotides used for plasmid construct preparation.

Table S4. Natural variation across elite cultivars.

Table S5. Natural variation across barley landraces.

Table S6. Natural variation across *Hordeum vulgare spontaneum* (wild barley).

Acknowledgements

We would like to thank Micha Bayer, Joanne Russell and Stylianos Kyriakidis for providing the data for the analysis of natural variation. We would like to thank Kath Wright, of the James Hutton Imaging Facility, for her assistance with the confocal microscopes and Dominika Lewandowska for assistance with antibodies. OMX microscopy was supported by the Euro-BioImaging PCS to IC and through the MRC Next Generation Optical Microscopy Award (Ref: MR/K015869/1) at the CAST Facility, University of Dundee. The research leading to these results has received funding from the European Community's Seventh Framework Programme FP7/2007–2013 (no. 222883), Biotechnology and Biological Science Research Council Grant BB/F020872/1, ERC Shuffle (Project ID: 669182) and the Scottish Government's Rural and Environment Science and Analytical Services Division work programme Theme 2 WP2.1 RD1 and RD2.

References

Able JA, Crismani W, Boden SA. 2009. Understanding meiosis and the implications for crop improvement. Functional Plant Biology **36,** 575–588.

Arnold K, Bordoli L, Kopp J, Schwede T. 2006. The SWISS-MODEL workspace: a web-based environment for protein structure homology modelling. Bioinformatics **22,** 195–201.

Baker K, Bayer M, Cook N, *et al*. 2014. The low-recombining pericentromeric region of barley restricts gene diversity and evolution but not gene expression. The Plant Journal **79,** 981–992.

Bannister LA, Pezza RJ, Donaldson JR, de Rooij DG, Schimenti KJ, Camerini-Otero RD, Schimenti JC. 2007. A dominant, recombination-defective allele of *Dmc1* causing male-specific sterility. PLoS Biology **5,** e105.

Barakate A, Higgins JD, Vivera S, *et al*. 2014. The synaptonemal complex protein ZYP1 is required for imposition of meiotic crossovers in barley. The Plant Cell **26,** 729–740.

Baudat F, Imai Y, de Massy B. 2013. Meiotic recombination in mammals: localization and regulation. Nature Reviews. Genetics **14,** 794–806.

Bishop DK, Park D, Xu L, Kleckner N. 1992. *DMC1*: a meiosis-specific yeast homolog of E. coli *recA* required for recombination, synaptonemal complex formation, and cell cycle progression. Cell **69,** 439–456.

Brown AH, Feldman MW, Nevo E. 1980. Multilocus structure of natural populations of *Hordeum spontaneum*. Genetics **96,** 523–536.

Carlton PM, Cande WZ. 2002. Telomeres act autonomously in maize to organize the meiotic bouquet from a semipolarized chromosome orientation. The Journal of Cell Biology **157,** 231–242.

Choi Y, Chan AP. 2015. PROVEAN web server: a tool to predict the functional effect of amino acid substitutions and indels. Bioinformatics **31,** 2745–2747.

Close TJ, Bhat PR, Lonardi S, *et al*. 2009. Development and implementation of high-throughput SNP genotyping in barley. BMC Genomics **10,** 582.

Colas I, Darrier B, Arrieta M, Mittmann SU, Ramsay L, Sourdille P, Waugh R. 2017. Observation of extensive chromosome axis remodeling during the "diffuse-phase" of meiosis in large genome cereals. Frontiers in Plant Science **8,** 1235.

Colas I, Macaulay M, Higgins JD, *et al*. 2016. A spontaneous mutation in MutL-Homolog 3 (HvMLH3) affects synapsis and crossover resolution in the barley desynaptic mutant *des10*. New Phytologist **212,** 693–707.

Colas I, Shaw P, Prieto P, Wanous M, Spielmeyer W, Mago R, Moore G. 2008. Effective chromosome pairing requires chromatin remodeling at the onset of meiosis. Proceedings of the National Academy of Sciences, USA **105,** 6075–6080.

Comadran J, Kilian B, Russell J, *et al*. 2012. Natural variation in a homolog of Antirrhinum CENTRORADIALIS contributed to spring growth habit and environmental adaptation in cultivated barley. Nature Genetics **44,** 1388–1392.

Couteau F, Belzile F, Horlow C, Grandjean O, Vezon D, Doutriaux MP. 1999. Random chromosome segregation without meiotic arrest in both male and female meiocytes of a *dmc1* mutant of *Arabidopsis*. The Plant Cell **11,** 1623–1634.

Da Ines O, Abe K, Goubely C, Gallego ME, White CI. 2012. Differing requirements for RAD51 and DMC1 in meiotic pairing of centromeres and chromosome arms in *Arabidopsis thaliana*. PLoS Genetics **8,** e1002636.

Da Ines O, Degroote F, Goubely C, Amiard S, Gallego ME, White CI. 2013. Meiotic recombination in Arabidopsis is catalysed by DMC1, with RAD51 playing a supporting role. PLoS Genetics **9,** e1003787.

Deng ZY, Wang T. 2007. OsDMC1 is required for homologous pairing in *Oryza sativa*. Plant Molecular Biology **65,** 31–42.

Devisetty UK, Mayes K, Mayes S. 2010. The *RAD51* and *DMC1* homoeologous genes of bread wheat: cloning, molecular characterization and expression analysis. BMC Research Notes **3,** 245.

Ding ZJ, Wang T, Chong K, Bai SN. 2001. Isolation and characterization of *OsDMC1*, the rice homologue of the yeast *DMC1* gene essential for meiosis. Sexual Plant Reproduction **13,** 285–288.

Doutriaux MP, Couteau F, Bergounioux C, White C. 1998. Isolation and characterisation of the *RAD51* and *DMC1* homologs from *Arabidopsis thaliana*. Molecular & General Genetics **257,** 283–291.

Druka A, Franckowiak J, Lundqvist U, *et al*. 2011. Genetic dissection of barley morphology and development. Plant Physiology **155,** 617–627.

Du L, Luo Y. 2013. Structure of a filament of stacked octamers of human DMC1 recombinase. Acta Crystallographica. **F69,** 382–386.

Etedali F, Baghban Kohnehrouz B, Valizadeh M, Gholizadeh A, Malboobi MA. 2011. Genome wide cloning of maize meiotic recombinase Dmc1 and its functional structure through molecular phylogeny. Genetics and Molecular Research **10,** 1636–1649.

Habu T, Taki T, West A, Nishimune Y, Morita T. 1996. The mouse and human homologs of *DMC1*, the yeast meiosis-specific homologous recombination gene, have a common unique form of exon-skipped transcript in meiosis. Nucleic Acids Research **24,** 470–477.

Harwood WA, Bartlett JG, Alves SC, Perry M, Smedley MA, Leyland N, Snape JW. 2009. Barley transformation using *Agrobacterium*-mediated techniques. In: Jones H, Shewry P, eds. Transgenic wheat, barley and oats. Methods In Molecular Biology (Methods and Protocols), Vol. **478**. Totowa, NJ, USA: Humana Press, 137–147.

Hernandes-Soriano JM. 1973. Desynaptic mutants in Betzes barley. Masters Thesis, University of Arizona.

Higgins JD, Perry RM, Barakate A, Ramsay L, Waugh R, Halpin C, Armstrong SJ, Franklin FC. 2012. Spatiotemporal asymmetry of the meiotic program underlies the predominantly distal distribution of meiotic crossovers in barley. The Plant Cell **24,** 4096–4109.

Himmelbach A, Zierold U, Hensel G, Riechen J, Douchkov D, Schweizer P, Kumlehn J. 2007. A set of modular binary vectors for the transformation of cereals. Plant Physiology **145,** 1192–1200.

Hockett EA, Eslick RF. 1969. Spontaneous frequencies of genetic and other sterilities in barley *Hordeum vulgare* L. Crop Science **9,** 23–24.

Hunter N. 2015. Meiotic recombination: the essence of heredity. Cold Spring Harbor Perspectives in Biology **7,** a016618.

International Barley Genome Sequencing Consortium, **Mayer KFX, Waugh R, *et al*.** 2012. A physical, genetic and functional sequence assembly of the barley genome. Nature **491,** 711–716.

Jacobsen J, Venables I, Wang M, Matthews P, Ayliffe M, Gubler F. 2006. Barley (*Hordeum vulgare* L.). In: Wang K, ed. Agrobacterium protocols, Vol. 1. Methods in Molecular Biology, Vol. 343. Totowa, NJ, USA: Humana Press, 171–183.

Jasencakova Z, Meister A, Schubert I. 2001. Chromatin organization and its relation to replication and histone acetylation during the cell cycle in barley. Chromosoma **110,** 83–92.

Jones GH, Franklin FC. 2006. Meiotic crossing-over: obligation and interference. Cell **126,** 246–248.

Kathiresan A, Khush GS, Bennett J. 2002. Two rice *DMC1* genes are differentially expressed during meiosis and during haploid and diploid mitosis. Sexual Plant Reproduction **14,** 257–267.

Keeney S, Bannister LA, Pezza RJ, Donaldson JR, de Rooij DG, Schimenti KJ, Camerini-Otero RD, Schimenti JC. 2007. A dominant, recombination-defective allele of *Dmc1* causing male-specific sterility. PLoS Biology **5,** e105.

Kinebuchi T, Kagawa W, Enomoto R, Tanaka K, Miyagawa K, Shibata T, Kurumizaka H, Yokoyama S. 2004. Structural basis for octameric ring formation and DNA interaction of the human homologous-pairing protein Dmc1. Molecular Cell **14,** 363–374.

Klimyuk VI, Jones JD. 1997. *AtDMC1*, the *Arabidopsis* homologue of the yeast *DMC1* gene: characterization, transposon-induced allelic variation and meiosis-associated expression. The Plant Journal **11,** 1–14.

Lambing C, Franklin FC, Wang CR. 2017. Understanding and manipulating meiotic recombination in plants. Plant Physiology **173,** 1530–1542.

Li J, Farmer AD, Lindquist I, Dukowic-Schulze S, Mudge J, Li T, Retzel EF, Chen C. 2012. Characterization of a set of novel meiotically-active promoters in *Arabidopsis*. BMC Plant Biology **12,** 104.

Li XC, Barringer BC, Barbash DA. 2009. The pachytene checkpoint and its relationship to evolutionary patterns of polyploidization and hybrid sterility. Heredity **102,** 24–30.

Lichten M, Brown MS, Grubb J, Zhang A, Rust MJ, Bishop DK. 2015. Small Rad51 and Dmc1 complexes often co-occupy both ends of a meiotic DNA double strand break. PLoS Genetics **11,** e1005653.

Liebe B, Petukhova G, Barchi M, *et al*. 2006. Mutations that affect meiosis in male mice influence the dynamics of the mid-preleptotene and bouquet stages. Experimental Cell Research **312,** 3768–3781.

Lin ZG, Kong HZ, Nei M, Ma H. 2006. Origins and evolution of the *recA/RAD51* gene family: Evidence for ancient gene duplication and endosymbiotic gene transfer. Proceedings of the National Academy of Sciences, USA **103,** 10328–10333.

Lorenz A, Mehats A, Osman F, Whitby MC. 2014. Rad51/Dmc1 paralogs and mediators oppose DNA helicases to limit hybrid DNA formation and promote crossovers during meiotic recombination. Nucleic Acids Research **42,** 13723–13735.

Lundqvist U, Franckowiak JD, Konishi T. 1997. New and revised descriptions of barley genes. Barley Genetics Newsletter **26,** 22–516.

MacQueen AJ. 2015. Catching a (double-strand) break: the Rad51 and Dmc1 strand exchange proteins can co-occupy both ends of a meiotic DNA double-strand break. PLoS Genetics **11,** e1005741.

Martinez-Perez E. 2009. Meiosis in cereal crops: the grasses are back. Genome Dynamics **5,** 26–42.

Mascher M, Gundlach H, Himmelbach A, *et al*. 2017. A chromosome conformation capture ordered sequence of the barley genome. Nature **544,** 427–433.

Mercier R, Mézard C, Jenczewski E, Macaisne N, Grelon M. 2015. The molecular biology of meiosis in plants. Annual Review of Plant Biology **66,** 297–327.

Mikhailova EI, Phillips D, Sosnikhina SP, Lovtsyus AV, Jones RN, Jenkins G. 2006. Molecular assembly of meiotic proteins Asy1 and Zyp1 and pairing promiscuity in rye (*Secale cereale* L.) and its synaptic mutant *sy10*. Genetics **174,** 1247–1258.

Nakashima M, Mimida N, Shimazu J, *et al*. 2004. Isolation and characterization of *OsDMC1*, the meiosis-specific recombinase gene from rice. Plant and Cell Physiology **45,** S202.

Passy SI, Yu X, Li Z, Radding CM, Masson JY, West SC, Egelman EH. 1999. Human Dmc1 protein binds DNA as an octameric ring. Proceedings of the National Academy of Sciences, USA **96,** 10684–10688.

Petersen G, Seberg O. 2002. Molecular evolution and phylogenetic application of DMC1. Molecular Phylogenetics and Evolution **22,** 43–50.

Petersen G, Seberg O, Yde M, Berthelsen K. 2006. Phylogenetic relationships of *Triticum* and *Aegilops* and evidence for the origin of the A, B, and D genomes of common wheat (*Triticum aestivum*). Molecular Phylogenetics and Evolution **39,** 70–82.

Phillips D, Nibau C, Wnetrzak J, Jenkins G. 2012. High resolution analysis of meiotic chromosome structure and behaviour in barley (*Hordeum vulgare* L.). PLoS One **7,** e39539.

Pittman DL, Cobb J, Schimenti KJ, Wilson LA, Cooper DM, Brignull E, Handel MA, Schimenti JC. 1998. Meiotic prophase arrest with failure of chromosome synapsis in mice deficient for *Dmc1*, a germline-specific RecA homolog. Molecular Cell **1,** 697–705.

Pradillo M, López E, Linacero R, Romero C, Cuñado N, Sánchez-Morán E, Santos JL. 2012. Together yes, but not coupled: new insights into the roles of RAD51 and DMC1 in plant meiotic recombination. The Plant Journal **69,** 921–933.

Russell J, Mascher M, Dawson IK, *et al*. 2016. Exome sequencing of geographically diverse barley landraces and wild relatives gives insights into environmental adaptation. Nature Genetics **48,** 1024–1030.

Sha L, Fan X, Yang R, Kang H, Ding C, Zhang L, Zheng Y, Zhou Y. 2010. Phylogenetic relationships between *Hystrix* and its closely related genera (Triticeae; Poaceae) based on nuclear *Acc1*, *DMC1* and chloroplast *trnL-F* sequences. Molecular Phylogenetics and Evolution **54,** 327–335.

Sheridan SD, Yu X, Roth R, Heuser JE, Sehorn MG, Sung P, Egelman EH, Bishop DK. 2008. A comparative analysis of Dmc1 and Rad51 nucleoprotein filaments. Nucleic Acids Research **36,** 4057–4066.

Shimazu J, Matsukura C, Senda M, Ishikawa R, Akada S, Harada T, Tabata S, Niizeki M. 2001. Characterization of a DMC1 homologue, RiLIM15, in meiotic panicles, mitotic cultured cells and mature leaves of rice (*Oryza sativa* L.). Theoretical and Applied Genetics **102,** 1159–1163.

Stolk L, Perry JR, Chasman DI, *et al*. 2012. Meta-analyses identify 13 loci associated with age at menopause and highlight DNA repair and immune pathways. Nature Genetics **44,** 260–268.

Sun G, Zhang X. 2011. Origin of the H genome in StH-genomic *Elymus* species based on the single-copy nuclear gene *DMC1*. Genome **54,** 655–662.

Volis S, Shulgina I, Zaretsky M, Koren O. 2011. Epistasis in natural populations of a predominantly selfing plant. Heredity **106,** 300–309.

Voorrips RE. 2002. MapChart: software for the graphical presentation of linkage maps and QTLs. The Journal of Heredity **93,** 77–78.

Wang H, Hu Q, Tang D, Liu X, Du G, Shen Y, Li Y, Cheng Z. 2016. OsDMC1 is not required for homologous pairing in rice meiosis. Plant Physiology **171,** 230–241.

Wang M, Wang K, Tang D, Wei C, Li M, Shen Y, Chi Z, Gu M, Cheng Z. 2010. The central element protein ZEP1 of the synaptonemal complex regulates the number of crossovers during meiosis in rice. The Plant Cell **22,** 417–430.

Voloshin ON, Wang L, Camerini-Otero RD. 1996. Homologous DNA pairing promoted by a 20-amino acid peptide derived from RecA. Science **272,** 868–872.

Yoshida K, Kondoh G, Matsuda Y, Habu T, Nishimune Y, Morita T. 1998. The mouse *RecA*-like gene *Dmc1* is required for homologous chromosome synapsis during meiosis. Molecular Cell **1,** 707–718.

Zhang XP, Galkin VE, Yu X, Egelman EH, Heyer WD. 2009. Loop 2 in *Saccharomyces cerevisiae* Rad51 protein regulates filament formation and ATPase activity. Nucleic Acids Research **37,** 158–171.